INTERNATIONAL JOURNAL OF ENERGY STUDIES

e-ISSN: 2717-7513 (ONLINE); homepage: https://dergipark.org.tr/en/pub/ijes

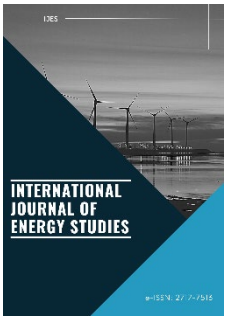

Research Article
Int J Energy Studies 2024; 9(4): 619-636
DOI: 10.58559/ijes.1552364

Received : 18 Sep 2024
Revised : 07 Oct 2024
Accepted : 14 Oct 2024

Experimental optimization of the SG6043 airfoil for horizontal axis wind turbine using Schmitz equations

Mehmet Seyhan[a], Himmet Erdi Tanürün[b*]

[a] *Department of Mechanical Engineering, Faculty of Engineering, Karadeniz Technical University, Trabzon, 61080, Türkiye, ORCID: 0000-0002-5927-9128*

[b]*Department of Energy Systems Engineering, Elbistan Faculty of Engineering, Kahramanmaraş Istiklal University, 46300, Türkiye, ORCID: 0000-0001-7814-7043*

*(*Corresponding Author: erdi.tanurun@istiklal.edu.tr)*

Highlights

- HAWT turbine blade was designed via Schmitz equations.
- Dynamic surface oil flow visualization successfully performed to elucidate the flow structure of the HAWT.
- C_P of M2 is superior to that of M1 at all TSR and RPM.

You can cite this article as: Seyhan M, Tanürün HE. Experimental optimization of the SG6043 airfoil for horizontal axis wind turbine using Schmitz equations. Int J Energy Studies 2024; 9(4): 619-636.

ABSTRACT

This study presents the experimental optimization of the SG6043 airfoil for horizontal axis wind turbines (HAWTs) using the Schmitz equation, focusing on enhancing power output and elucidating the surface flow structure. Two blade models, M1 (conventional) and M2 (optimized), were designed and tested at rotational speeds of 400 rpm and 600 rpm across a range of tip speed ratios (TSR). The M2 model, optimized using Schmitz equations, demonstrated significantly improved performance compared to the M1 model at both rotational speeds. At 400 rpm, the maximum power coefficient (C_P) for M1 was 0.274, while M2 reached 0.419, indicating a 52.91% improvement. At 600 rpm, M1 achieved a maximum C_P of 0.293, whereas M2 attained 0.458, representing a 56.31% enhancement. The M2 model also showed superior performance at higher TSRs, with the highest percentage increase in C_P recorded at 4.9 TSR, reaching 574.54%. Additionally, dynamic surface oil-flow visualization experiments were conducted to examine flow behavior on the blade surfaces. Results indicated better flow attachment in the M2 blade due to its optimized twist angle and chord length, particularly in the mid-section, leading to delayed flow separation. The reattachment observed on the suction side of the M2 model, following the laminar separation bubble (LSB), which was absent in the M1, contributed to its higher aerodynamic efficiency and overall power performance. These findings confirm that the optimized SG6043 airfoil design, guided by Schmitz equations, offers significant improvements in HAWT performance, particularly under varying operational conditions.

Keywords: Horizontal axis wind turbine, Schmitz theory, Rotor blade design, Experimental

1. INTRODUCTION

In contemporary society, energy has become an indispensable requirement, with global demand continuously escalating. Since the Industrial Revolution, fossil fuels have served as the predominant energy source, underpinning the vast majority of energy production processes [1,2]. However, the combustion of fossil fuels results in the emission of greenhouse gases, contributing significantly to atmospheric pollution, which poses severe threats to public health and disrupts ecological balances [3-4]. The degradation of the ozone layer due to these emissions exacerbates the harmful effects of solar radiation, thereby increasing the risks to biological systems. Moreover, the finite nature of fossil fuel reserves introduces volatility in energy markets, with fluctuations in supply and demand leading to increased costs [5].

The aforementioned environmental and economic drawbacks of fossil fuels have necessitated the exploration and adoption of alternative energy sources. In this regard, renewable energy technologies, including solar, geothermal, biomass, and particularly wind energy, have gained substantial attention [6,7]. These renewable sources are not only inherently sustainable due to their reliance on inexhaustible natural resources, but they also offer significant environmental advantages, such as reduced greenhouse gas emissions [8]. Among renewable energy technologies, wind energy stands out, especially with the advent and optimization of horizontal-axis wind turbines (HAWTs), which have demonstrated high efficiency and a broad range of applicability in various energy sectors. HAWTs, through their aerodynamic and structural advancements, have become pivotal in maximizing the energy capture from wind resources, thereby contributing significantly to the transition towards a more sustainable energy future.

When oriented perpendicularly to the wind flow, the blades generate aerodynamic lift, leading to rotation [9]. The design of HAWTs results in higher efficiency compared to veritcal-axis wind turbines (VAWTs), as it allows for continuous energy extraction throughout the full rotational cycle of the blades, especially under stable wind conditions. Furthermore, HAWTs are unaffected by the backtracking effect [10]. For HAWTs, various optimization objectives can be pursued, such as maximizing aerodynamic efficiency, reducing structural weight, minimizing fatigue loads, lowering noise levels, and cutting costs, all of which contribute to enhancing overall performance and reliability.

In recent times, there has been an increasing focus in the literature on HAWTs blades, particularly on how different design modifications and optimization strategies can enhance their energy capture efficiency, leading to improved performance and broader commercial adoption. Kim et al. conducted a study that demonstrated how modifying the leading edge (LE) and trailing edges (TE) of airfoils can significantly impact the aerodynamic performance and power (P) production of HAWTs, with findings showing that the S809r airfoil with a more rounded LE increased P output by 2.3 times, and the S809gx airfoil by 2 times [11]. The literature presents the Blade Element Momentum (BEM) method as a primary integral method for conducting aerodynamic analysis around HAWT rotors and optimizing blade design. This method is particularly effective in assessing the impact of twist angle (θ) and chord length (c) variations, leading to highly efficient rotor performance. To initiate the blade design process, the Schmitz theory is used, providing an initial blade configuration. Following this, the BEM theory is applied to calculate the forces (F), torque (T), and P extracted by the turbine, enabling further optimization of the blade geometry [12-13]. Zidane et al. conducted a study using CFD-BEM modeling and neural networks, revealing that under sandstorm conditions, the P output of large-scale HAWTs can decrease by up to 30% due to aerodynamic losses, and developed a model to predict erosion rates on turbine blades as a function of debris flow rate, Reynolds number (Re), and angle of attack (α) [14]. Bouhelal et al. developed and validated a machine learning-based approach, integrating an optimized Artificial Neural Network (ANN) with the BEM theory, which efficiently predicts aerodynamic performance of wind turbine rotors, demonstrating accuracy with over $2x10^{13}$ training data points and offering a rapid alternative for cases where airfoil data is unavailable [15]. Hamlaoui et al. developed a novel stall delay model for small HAWT blades, improving the prediction of 3D lift coefficients (C_L) by correcting 2D lift data, with results showing enhanced accuracy in P and T predictions when validated against NASA Ames wind tunnel data and NREL Phase VI turbine measurements [16]. Bouhelal et al. conducted a comparative study between BEM and CFD-RANS methods for predicting HAWT performance, finding that while BEM underestimates normal Fs and overestimates tangential Fs—leading to a T overprediction of over 30% at high wind speeds—CFD-RANS demonstrated uniform accuracy across all flow conditions, particularly in capturing flow separation [17]. Mansi and Aydın developed a new blade profile with a fixed TE flap for small-scale HAWTs, showing through BEM analysis and CFD validation that the modified design increased the power coefficient (C_P) by 8.3% and annual energy yield to 6944 kWh, with CFD predicting a 14% higher power coefficient than BEM [18]. Abdelsalam et al. developed and experimentally validated a new linearized rotor blade design for small-scale HAWTs, achieving a

$C_{P,max}$ of 0.426 at a tip-speed ratio (TSR or λ) of 5.1 and a 10 m/s wind speed, while reducing blade volume by 26% compared to a classical rotor, demonstrating superior performance at lower wind speeds [19]. Wang et al. optimized the local θs of wind turbine blades using a kriging surrogate model, achieving a 4.83% increase in wind C_P for the NREL Phase VI blade and 3.44% for the WindPACT blade, though with increased structural loads on the optimized blades [20]. Akbari et al. optimized the c and θ of a small wind turbine blade using a genetic algorithm, resulting in a 140% increase in startup T and a reduction in startup wind speed from 6 m/s to 4 m/s, with only a 1.5% decrease in C_P compared to the base blade [21]. Siram et al. designed and tested four small-scale HAWT models using BEM theory and wind tunnel experiments, finding that the M1 rotor, composed of an E216 airfoil, achieved the $C_{P,max}$ of 0.34 at 9 m/s, which is 92% of the BEMT prediction, demonstrating superior performance compared to the other rotors [23]. Rodriguez and Celis developed a hybrid CFD/BEM/GA methodology for optimizing the blade design of a 5 kW HAWT, achieving a $C_{P,max}$ of 0.4658 at TSR of 6, with the optimized airfoil demonstrating a C_L of 1.2437 and a lift-to-drag ratio (C_L/C_D) of 67.36 at an $\alpha = 5.55°$ [23]. Jha et al. extended the BEM theory to account for wake effects in small-scale HAWT blade design, selecting the SG6043 airfoil for its high spanwise ratio, and demonstrated that the designed blade closely matches experimental results and efficiently maximizes P even at low wind speeds [24]. Tokul and Kurt, in their study comparing NACA 6409 and NACA 2414 airfoils using the BEM, demonstrated that NACA 6409, with a 4% higher camber ratio and 5% lower thickness ratio, achieved a higher C_L and greater energy production, particularly at a wind speed of 10 m/s, where NACA 6409 outperformed NACA 2414 in energy generation [25]. However, while there are numerous studies involving the BEM theory, there is no existing research that specifically examines the effect of the Schmitz equations in optimizing the SG6043 airfoil in an experimental setting.

Originality of the present experimental study is to elucidate surface flow structure of the turbine blade via dynamic surface oil flow visualization experiment and evaluate the performance of variation on HAWT with optimized and unoptimized turbine blade design. The main contributions of the present study are elucidation of the surface flow structure on turbine blade via dynamic surface oil flow visualization method and optimized blade design via Schmitz Equations by comparing unoptimized blade. Turbine blades with SG6043 airfoil are designed designed using Schmitz equation, optimizing critical parameters such as twist angle (θ) and chord (c). The optimized turbine blade having SG6043 airfoil profile is then compared to the simple turbine blade having SG6043 model. This comprehensive approach aims to provide new insights into the turbine

blade design via Schmitz by contributing the advancement of wind turbine blade design methodologies and elucidating surface flow structure around the designed turbine blade.

2. EXPERIMENTAL SETUP

The experimental setup consists of 3 sub-section that are blade design, torque measurement and dynamic surface oil flow visualization.

2.1. Blade Design

In HAWT, blade design plays a critical role for turbine performance [26]. The aerodynamic characteristics of the turbine blade, such as lift and drag coefficient, depend on the type of airfoil. Therefore, blades with high aerodynamic efficiency are used in turbine blade design [27]. In this regards, it is an important parameter that the airfoil selected for the efficiency of the turbine has a high L/D ratio in turbine blade design [26]. Considering this criterion, the SG6043 airfoil profile, has a high L/D ratio designed by Giguere and Selig [28] for small-scale horizontal axis wind turbines and this airfoil has been studied in the literature on the aerodynamic performance HAWTs [29-31]. Therefore SG6043 airfoil profile was selected to design the turbine blade via Schmitz equations.

Determination of the blade's chord length and twist angle distribution, selection of the airfoil, number of blades and design λ constitute the basic aerodynamic design parameters of the wind turbine rotor. Table 1 lists the design parameters for the blades optimization. In order to determine the design lift coefficient $(C_L)_D$, the study by Singh et al. [30] at Re of 100,000 was taken as reference. According to this study, the maximum C_L of the SG6043 airfoil at the optimum angle was found to be 1.26. It is seen that the design α is 6° for the case where the L/D ratio is maximum. In addition, the design tip speed ratio of 4 was selected. Manwell et al. [32] suggested 3-4 wind turbine blades for a speed ratio of 4. The rotor radius for the turbine was determined as 0.45 m.

Table 1. The design parameters of HAWT rotor blade

Parameters	Values
Design tip speed ratio, λ_D	4
Rotor radius, R	0.45 m
Blade number, B	3
Design angle of attack, α_D	6 °
Design lift coefficient, $(C_L)_D$	1.26
Airfoil type	SG6043

In turbine blade design, formulas such as Betz and Schmitz are the methods used to obtain the optimum blade geometry [33]. According to Betz, no wake rotation or drag is assumed to provide maximum power from the turbine blade [32]. The Betz method is ideal for wind turbine blade design, but more advanced optimisation methods are often used in practice [34]. As a result, it is more appropriate to design the optimum horizontal axis wind turbine blade according to Schmitz formulas. Therefore, in this study, the datas for the variation of the chord lengths and twist angles along the blade for the optimum turbine blade geometry are obtained from Schmitz formulas.

The following equations are used to obtain optimum horizontal axis wind turbine blade. Among the designed blades, the model designed by using Schmitcs equation is named as M1 and the model designed by using the section 1 and section 10 values (chord and twist angles) calculated in this equation is named as M2. The blade is divided into 10 sections as seen in Figure 1 for M2 and the chord length and twist angle in each section can be found as follows,

$$c(r) = \frac{16\pi r}{B(C_L)_D} sin^2\left(\frac{1}{3} arctan\left(\frac{R}{r\lambda_D}\right)\right) \quad (1)$$

$$\theta(r) = \frac{2}{3} arctan\left(\frac{R}{r\lambda_D}\right) - \alpha_D \quad (2)$$

where R is rotor radius, r is blade section radius, $(C_L)_D$ is design lift coefficient, λ_D is design tip speed ratio, B is blade number and α_D is design angle of attack respectively. The data of chord lengths and twist angles thus obtained are given in Table 2 and Figure 1.

Table 2. Chord lengths and twist angles at different sections for optimum wind turbine blade

Section No	Blade section radius, r (m)	Chord, c (m)	Twist Angle, θ (°)
1	0.045	0.0893	39.466
2	0.09	0.1036	28.227
3	0.135	0.0945	20.537
4	0.180	0.0820	15.337
5	0.225	0.0709	11.710
6	0.270	0.0618	9.080
7	0.315	0.0545	7.103
8	0.360	0.0486	5.569
9	0.405	0.0438	4.349
10	0.450	0.0398	3.357

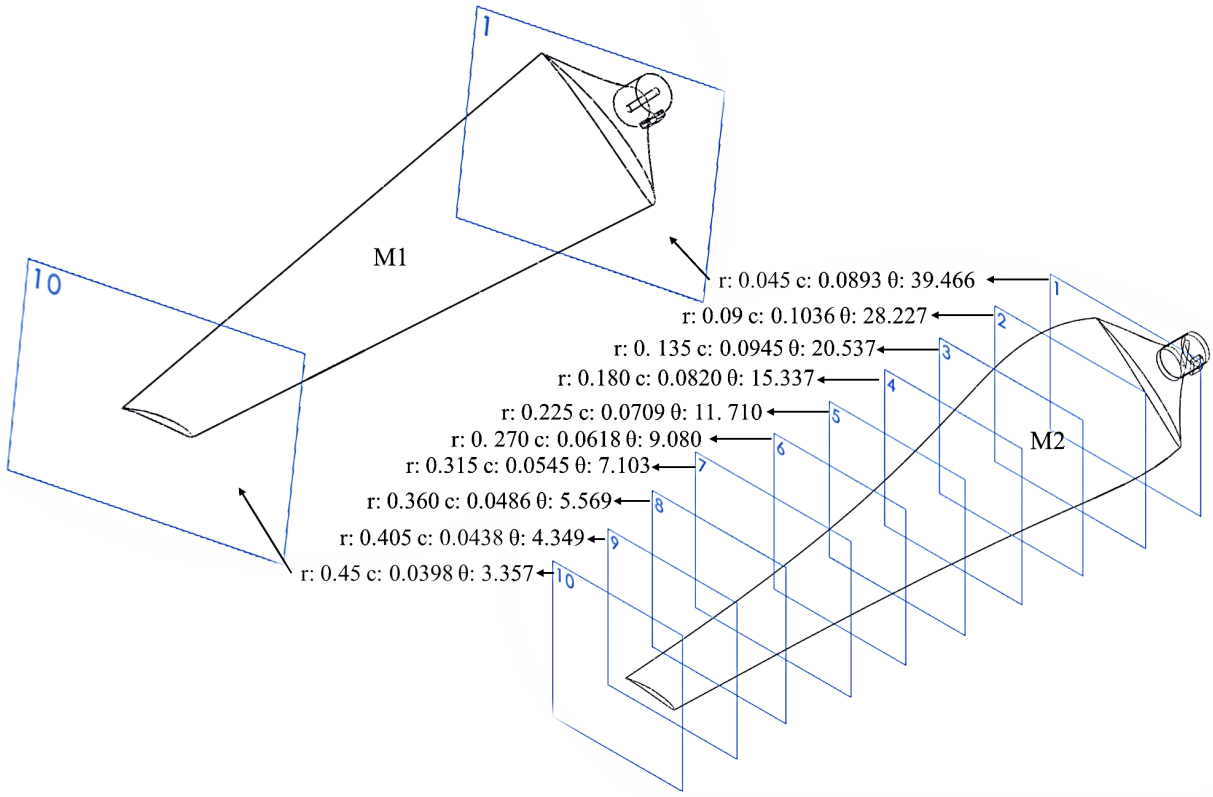

Figure 1. Schematic view of the design HAWT blades for M1 and M2

The designed M1 and M2 models were produced using a 3D printer, as seen in Figure 2. The surface of these blade models was made smooth by applying putty and then sanding.

2.2. Torque Measurement

The power coefficent measurements of the 3-blade small scale HAWT developed using the designed M1 and M2 blade models were carried out in a blown type wind tunnel. The general view of the torque measurement experimental setup is given in Figure 2. The torque measurement system consists of a hysterisis brake, a rotary torque device, a 3-bladed turbine rotor and blowing type wind tunnel. Magtrol HB-450M-2 hysteresis brake was used to measure the torque from the rotary torque device. GW Instek 3323 power supply was utilized to load the hysterisis brake that allowing to measure turbine torque at the rotary torque device. This torque device can measure torque and turbine rotational speed up to 5 Nm and 15000 *rpm*, respectively. The blowing type wind tunnel has 1.25 m x 1.25 m sqaure test section and can provide free stream velocity changing between 0 and 11 m/s. In the open test section, the wind speed can be precisely adjusted to the desired speed with the help of a frequency inverter. Rotary torque measurement was performed at

constant angular velocity. To do this, the braking mechanism (via Magtrol HB-450M-2 hysteresis brake) used to keep the rotation speed of the HAWT turbine rotor while increasing the free-stream velocity. Each torque measurement was taken for 75 seconds with 20 torque data per second from the torque device.

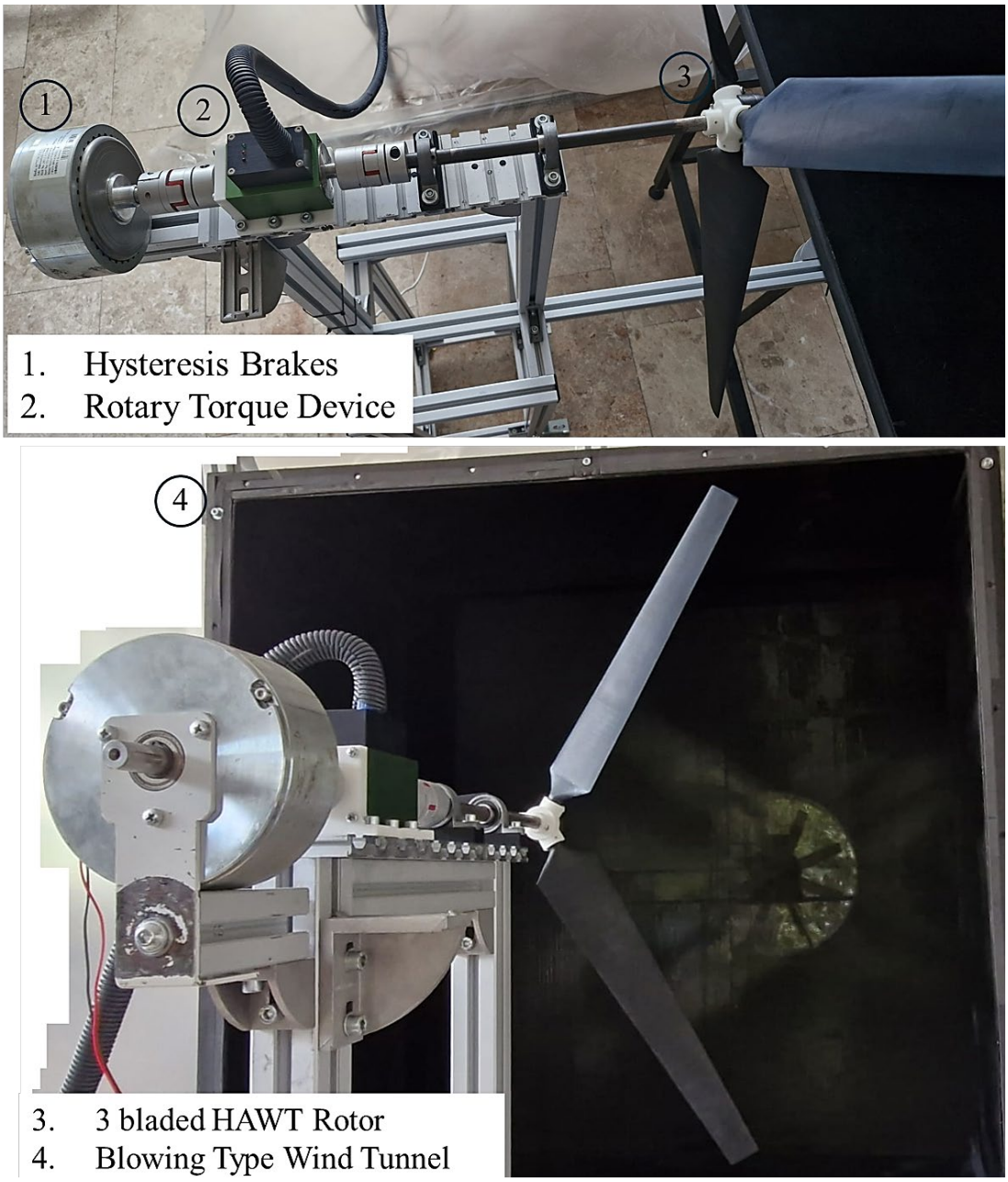

Figure 2. Experimental setup of dynamic torque measurement for 3 bladed HAWT for M1 and M2

The C_T and C_P values were obtained from Equations 3-4, based on the measured torque [35].

$$T = \frac{1}{2} C_T \rho A R U_0^2 \quad (3)$$

$$C_P = C_T * \lambda \quad (4)$$

C_T represents the torque coefficient, ρ denotes the density and A represents the swept area. The λ or TSR term in Equation 5 is explained in Equation 5 [36].

$$\lambda = \frac{R\omega}{U_O} \quad (5)$$

where, ω is defined as the rotation speed of the wind türbine.

2.3. Dynamic Surface Oil Flow Visualization

A dynamic surface oil flow visualization experiments was carried out to obtain the flow structure around the turbine blade during rotation of the 3-blade HAWT models. The mixture to be used in the oil flow visualization experiment consists of titanium dioxide, oleic acid and kerosene in a ratio of 1:5:7, respectively. This mixture was applied to both suction and pressure surfaces of the turbine blade. For M1 and M2 model, each experiment was performed at 600 *rpm* for approximately 30 minutes. Images of the flow structures formed on the turbine blade surface were captured using a GoPro Hero 7 black camera.

3. RESULTS AND DISCUSSION

The power performance of a novel M2, developed using the Schmitz equation, has been experimentally compared with a conventional M1 model at two different rotational speeds. The experiments were conducted at 400 *rpm* and 600 *rpm*, across a range of TSRs. Figure 3.a and 3.b, respectively, present the C_P and percentage enhanced C_P performance graphs for the M1 and M2 HAWT models at 400 *rpm*, based on dynamic torque measurements at different TSRs (M1= 2.8-4.6 λ and M2= 3.4-6.3 λ). The fact that each model operates at different TSRs results from obtaining more accurate and stable C_P values at the specified TSR ranges. The findings also reveal that the M2 model consistently outperforms the M1 model across all TSRs, with the performance improvement becoming more pronounced as the TSRs increase. When comparing the $C_{P,max}$ values of the M1 and M2 models, they were found to be 0.274 and 0.419, respectively, indicating a 52.91% improvement in performance. The λ range where both models were measured

simultaneously is between 3.4 and 4.5, as the M1 model was unable to generate any torque beyond a TSR of 4.5, resulting in no observable power coefficient. Within the λ range from 3.4 to 4.5, the power coefficient of the M2 model increased in a parabolic manner compared to the M1 model, with the highest enhanced C_P recorded at 4.5 λ, reaching a 361% improvement.

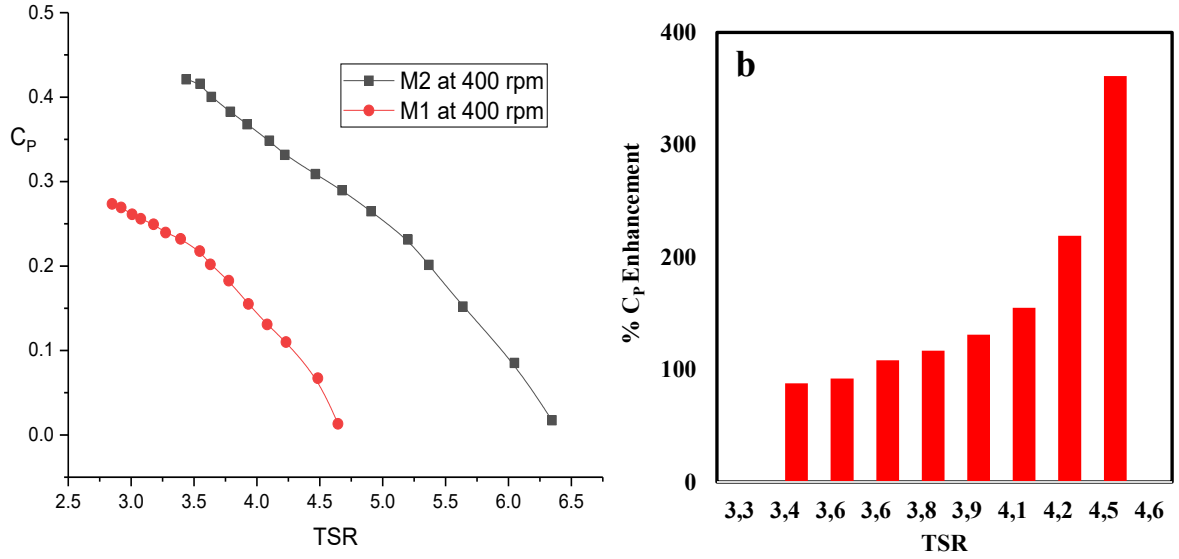

Figure 3. C_P performance for M1 and M2 HAWT models at 400 *rpm*: a) C_P, b) Percentage enhanced C_P at different TSRs

Figure 4.a and 4.b, respectively, present the C_P and percentage enhanced C_P performance graphs for the M1 and M2 HAWT models at 400 *rpm* at different TSRs (M1 = 2.7-5 λ and M2 = 3.4-7.8 λ). Similar to the results observed at 400 *rpm*, the M2 model consistently demonstrated significantly higher performance than the M1 model at 600 *rpm* across all TSRs. Furthermore, the maximum C_P for the M1 model was recorded as 0.293 at a λ of 3.1, while for the M2 model, it was 0.458 at a λ of 4.2, indicating a 56.31% improvement over the M1 model. On the other hand, both models were only compared within the TSR range of 3.5 to 4.9. As was the case at 400 *rpm*, the effect of the Schmitz equation became more pronounced with increasing TSRs at 600 *rpm*, with the M2 model showing a 574.54% performance increase over the M1 model at a λ of 4.9.

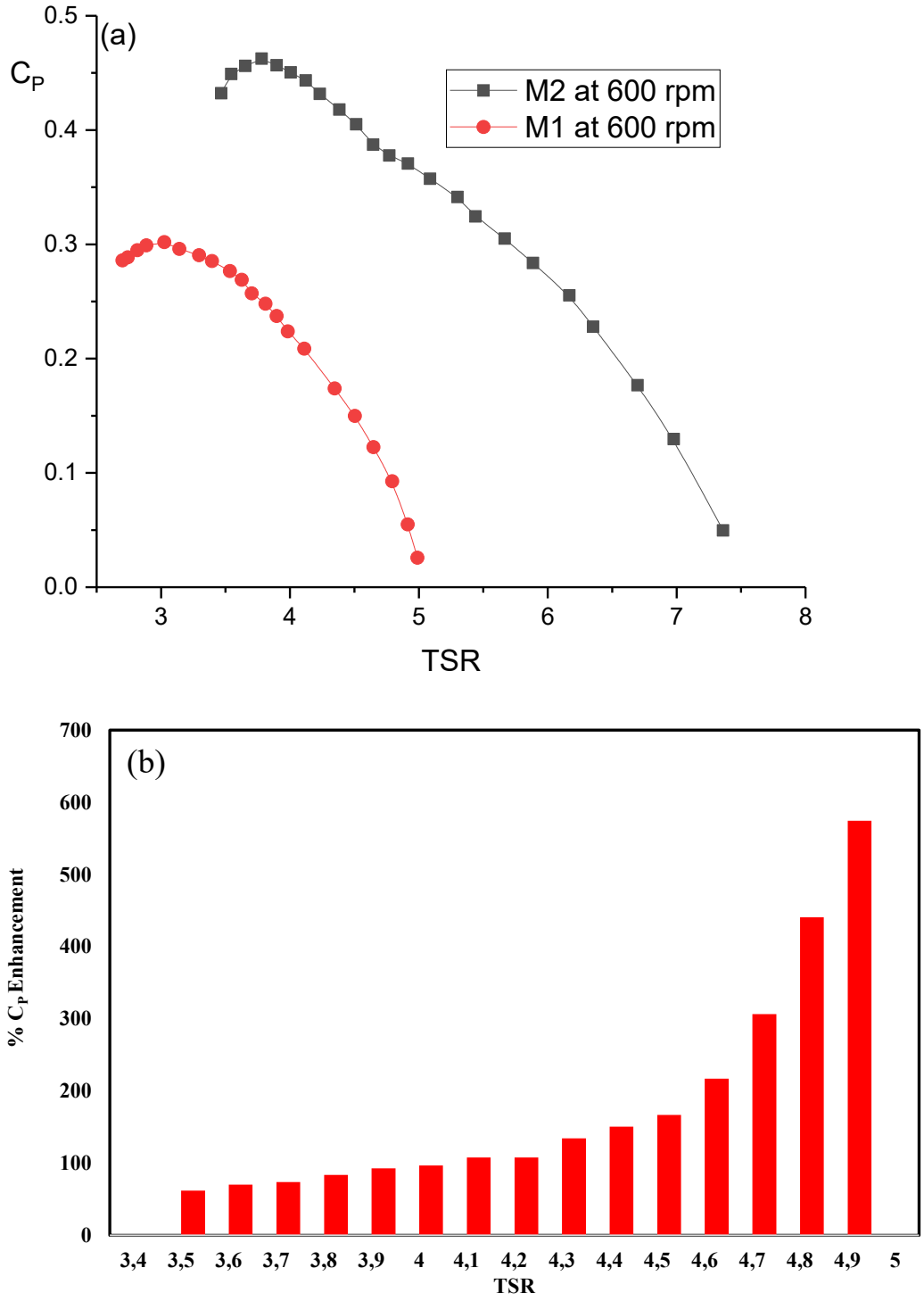

Figure 4. C_P performance for M1 and M2 HAWT models at 400 *rpm*: a) C_P, b) Percentage enhanced C_P at different TSRs

At both rotational speeds, the traditional blade failed to generate torque at higher TSRs, resulting in no measurable power coefficient, while the optimal model continued to generate power at higher TSRs. This indicates that the blade profile designed with the Schmitz equation enables HAWTs to

maintain power output even in conditions of high wind speeds.This suggests that the optimized blade geometry, guided by the Schmitz equation, enhances the overall efficiency and energy capture capability of the turbine under various operational conditions.

In the study of Chen and Liou [37], they investigated the variation of C_P with respect to TSR by varying the pitch angle (β) of turbine blade (that indicates the incident angle of incoming flow to blades) between 5° and 25° instead of designing the optimal turbine blade. As seen in Figure 5, they have shown that C_P of the HAWT increases spectacularly with the decrease of the pitch angle of the blades. Similarly, in the study of Hsiao et al. [38], there is a significant difference between the C_P values of optimum blade design (OPT) and unoptimized turbine blade (UnOPT) models as shown in Figure 5. This difference between optimized and unoptimized turbine blade is due to stall situation especially in unoptimized turbine blade. As can be concluded from Figures 5, these increases in turbine performance are not surprising when the turbine blade is optimized as it was in the present study.

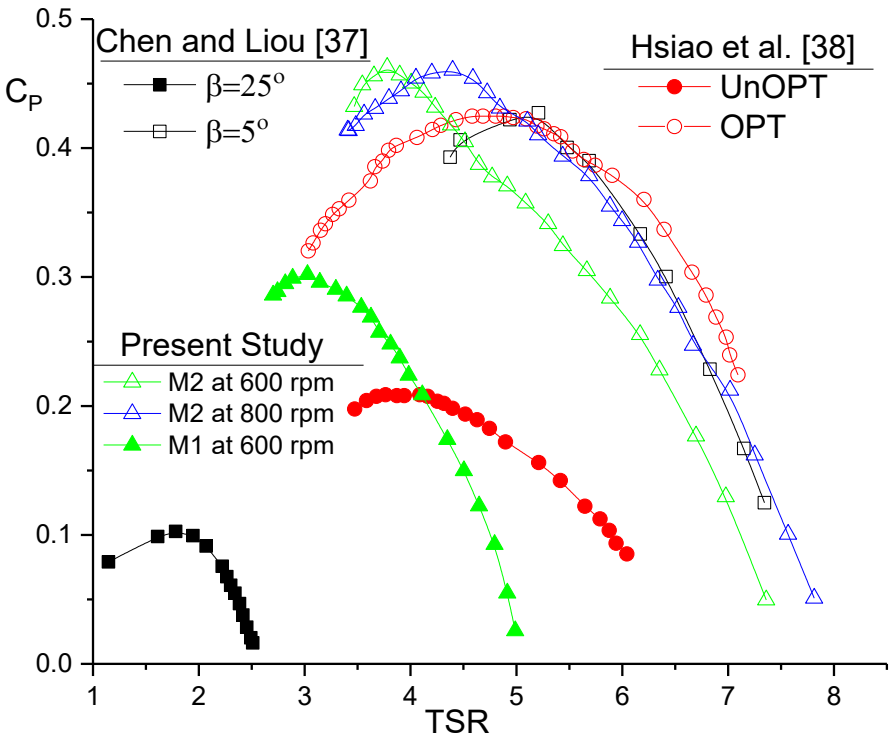

Figure 5. C_P – TSR results of the present study compared with Chen and Liou [37] and Hsiao et al. [38]

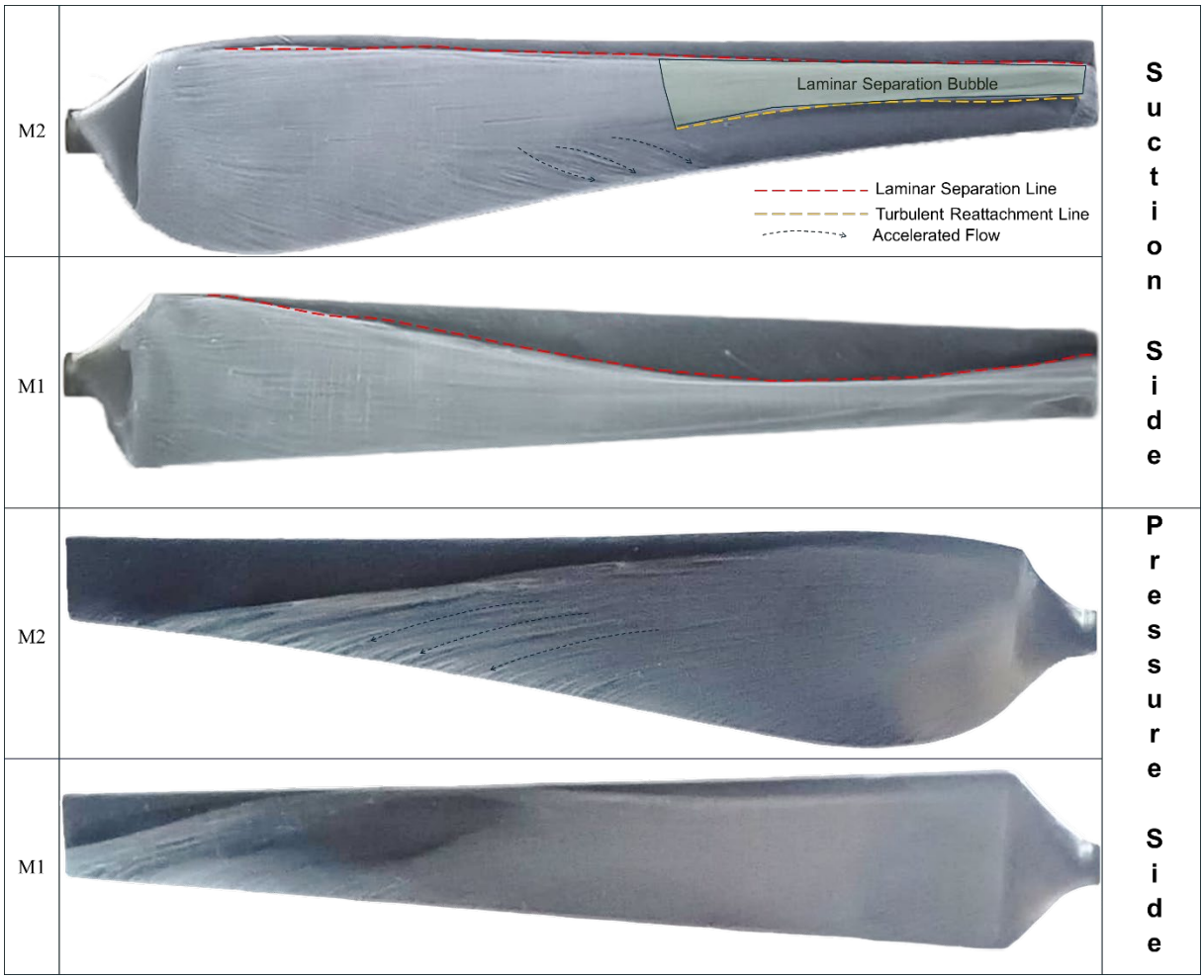

Figure 6. Surface oil-flow visualizations of the M1 and M2 at 600 *rpm*

In Figure 6, the dynamic surface oil-flow visualizations at a λ of 3.9 for the M1 and M2 models at 600 *rpm* are shown in two regions: suction and pressure region. In both blade models, flow separation occurred at the root-section, as indicated by the thick layer of oil, which is an expected outcome. This is due to the low angular velocity in the root region, resulting in reduced kinetic energy. In both the M1 and M2 blades, the flow in the root region lacks sufficient momentum to overcome the adverse pressure gradient, leading to early boundary layer separation. On the pressure and suction surfaces of the M2 blade, an accelerated flow from the root-section towards the mid-section region, caused by centrifugal acceleration, is observed, indicating that the flow remains attached to the blade surface in this region. However, this attachment at the mid-section, seen in the M2 blade, is not observed in the M1 blade. This difference is attributed to the varying twist angles along the spanwise, which is a result of the Schmitz equation's influence on the blade design. For the M1 blade, after flow separation occurs in approximately 50% of the mid-section and 20% of the tip-section, no reattachment of the flow is observed along the rest of the blade. A

laminar separation bubble (LSB) refers to a flow phenomenon where laminar flow separates from the airfoil surface due to an adverse pressure gradient but reattaches after a short distance. In the M2 blade, however, the flow remains attached along the leading edge throughout the spanwise, maintaining laminar flow. From the mid-section to the tip-section, an LSB forms over approximately 20% to 50% of the surface. After this, reattachment occurs around the middle of the blade, with the flow remaining attached up to the trailing edge. Notably, no trailing edge flow separation (TEFS) is observed in the mid-section or tip-section of the M2 blade. The reattachment observed in the mid-section of the M2 blade, which does not occur on the M1 blade surface, as shown in Figure 4.a at 3.9 TSR, serves as evidence for the higher power coefficient exhibited by the M2 blade. When evaluating the pressure side, it is observed that in the M2 blade, the flow begins to attach to the surface in a region between the root and mid-section. This attached flow progressively expands towards the tip, with the entire surface at the tip-section exhibiting fully attached flow. On the pressure side of the M1 blade, the flow begins to attach between the mid-section and the tip region; however, no region, including the tip, exhibits fully attached flow across the entire surface. When examined overall, suction and pressure region of in the M2 model, the flow remains more attached to the blade surface, indicating better aerodynamic performance, while in the M1 model, flow separation occurs earlier along the blade, leading to a less efficient flow structure. This suggests that the optimized blade geometry of the M2 model, influenced by the Schmitz equation, allows for better control of the boundary layer and delayed flow separation, which contributes to its superior performance at higher TSRs.

4. CONCLUSION

In this study, the aerodynamic performance of two HAWT blade models, M1 and M2, was experimentally compared, with the M2 model being optimized using the Schmitz equation. Through extensive testing at different TSR values and rotational speeds, the optimized blade geometry of the M2 model consistently demonstrated superior performance over the M1 model. The findings highlight the effectiveness of the Schmitz equation in optimizing blade geometry for enhanced energy capture and efficiency under various operational conditions.

- The M2 model outperformed the M1 model at both 400 rpm and 600 rpm across all TSR values, showing a maximum improvement in power coefficient of 56.31% at 600 rpm and 52.91% at 400 rpm.

- Flow visualization revealed that the M2 model maintained better flow attachment along the blade surface, particularly on the suction side, with a laminar separation bubble (LSB) reattaching to the surface, contributing to enhanced aerodynamic efficiency.
- The optimized blade geometry in the M2 model, influenced by the Schmitz equation, led to delayed flow separation and better boundary layer control, resulting in superior performance, especially at higher TSR values.
- The findings suggest that using the Schmitz equation for blade optimization in HAWTs can improve energy capture efficiency, even in conditions of high wind speeds, making it a valuable method for designing more efficient wind turbines.

ACKNOWLEDGMENT

If available, any institution, company, and etc. that supports to the paper submitted should be acknowledged here.

DECLARATION OF ETHICAL STANDARDS

The authors of the paper submitted declare that nothing which is necessary for achieving the paper requires ethical committee and/or legal-special permissions.

CONTRIBUTION OF THE AUTHORS

Mehmet Seyhan: Writing – review & editing, Writing – original draft, Validation, Resources, Methodology, Investigation, Formal analysis, Data curation, Conceptualization.

Himmet Erdi Tanürün: Writing – review & editing, Writing – original draft, Validation, Methodology, Investigation, Formal analysis, Data curation, Conceptualization.

CONFLICT OF INTEREST

There is no conflict of interest in this study.

REFERENCES

[1]Akuru UB, Onukwube IE, Okoro OI, Obe ES. Towards 100% renewable energy in Nigeria. Renewable and Sustainable Energy Reviews 2017 ;71 :943-953.

[2]Kuşkaya S, Bilgili F. The wind energy-greenhouse gas nexus: The wavelet-partial wavelet coherence model approach. Journal of Cleaner Production 2020; 245; 118872.

[3]Chen WH, Chen CY, Huang CY, Hwang CJ. Power output analysis and optimization of two straight-bladed vertical-axis wind turbines. Applied Energy 2017;185:223-232.

[4]Paçacı Ç. Hybrid axis wind turbine profile design. International Journal of Energy Studies. 2024 ;9(1) :1-19.

[5]Tanürün HE. Improvement of vertical axis wind turbine performance by using the optimized adaptive flap by the Taguchi method. Energy Sources, Part A: Recovery, Utilization, and Environmental Effects 2024; 46(1): 71-90.

[6]Avtar R, Sahu N, Aggarwal AK, et al. Exploring renewable energy resources using remote sensing and GIS-A review. Resources 2019; 8(3).

[7]Çakıroğlu R, Tanürün HE, Acır A, Üçgül F, Olkun S. Optimization of NACA 4412 augmented with a gurney flap by using grey relational analysis. Journal of the Brazilian Society of Mechanical Sciences and Engineering 2023; 45(3) :1-18.

[8]Li J, Wang G, Li Z, Yang S, Chong WT, Xiang X. A review on development of offshore wind energy conversion system. International Journal of Energy Research 2020;44(12):9283-9297.

[9]Johari MK, Jalil MAA, Shariff MFM. Comparison of horizontal axis wind turbine (HAWT) and vertical axis wind turbine (VAWT). International Journal of Engineering and Technology(UAE) 2018; 7(4) :74-80.

[10] Shires A, Kourkoulis V. Application of Circulation Controlled Blades for Vertical Axis Wind Turbines. Energies 2013; 6(8): 3744-3763.

[11] Kim Y, Bangga G, Delgado A. Investigations of HAWT Airfoil Shape Characteristics and 3D Rotational Augmentation Sensitivity Toward the Aerodynamic Performance Improvement. Sustainability 2020; 12(18): 7597.

[12] Hamlaoui MN, Bouhelal A, Smaili A, Khelladi S, Fellouah H. An inverse CFD actuator disk method for aerodynamic design and performance optimization of Horizontal Axis Wind Turbine blades. Energy Conversion Managment 2024; 316: 118818.

[13] Al-Abadi A, Ertunç Ö, Beyer F, Delgado A. Torque-Matched Aerodynamic Shape Optimization of HAWT Rotor. Journal of Physics: Conference Series 2014; 555(1): 012003.

[14] Zidane IF, Swadener G, Ma X, Shehadeh MF, Salem MH, Saqr KM. Performance of a wind turbine blade in sandstorms using a CFD-BEM based neural network. Journal of Renewable and Sustainable Energy 2020; 12(5).

[15] Bouhelal A, Ladjal A, Smaili A. Blade Element Momentum Theory Coupled with Machine Learning to Predict Wind Turbine Aerodynamic Performances. AIAA SCITECH, 2023; 23; 1153.

[16] Hamlaoui MN, Smaili A, Fellouah H. Improved BEM Method for HAWT Performance Predictions. International Conference on Wind Energy and Applications in Algeria, (ICWEAA); Algiers, Algeria, 2018.

[17] Bouhelal A, Smaili A, Guerri O, Masson C. Comparison of BEM and Full Navier-Stokes CFD Methods for Prediction of Aerodynamics Performance of HAWT Rotors. International Renewable and Sustainable Energy Conference (IRSEC), Taniger, Morocco, 2017.

[18] Mansi A, Aydin D. The impact of trailing edge flap on the aerodynamic performance of small-scale horizontal axis wind turbine. Energy Conversion Managment 2022; 256: 115396.

[19] Abdelsalam AM, El-Askary WA, Kotb MA, Sakr IM. Experimental study on small scale horizontal axis wind turbine of analytically-optimized blade with linearized chord twist angle profile. Energy 2021; 216: 119304.

[20] Wang H, Jiang X, Chao Y, et al. Numerical optimization of horizontal-axis wind turbine blades with surrogate model 2020; 235(5): 1173-1186.

[21] Akbari V, Naghashzadegan M, Kouhikamali R, Afsharpanah F, Yaïci W. Multi-Objective Optimization of a Small Horizontal-Axis Wind Turbine Blade for Generating the Maximum Startup Torque at Low Wind Speeds. Machines 2022; 10(9): 785.

[22] Siram O, Kesharwani N, Sahoo N, Saha UK. Aerodynamic Design and Wind Tunnel Tests of Small-Scale Horizontal-Axis Wind Turbines for Low Tip Speed Ratio Applications. Jornal Solar Energy Engineering 2022; 144(4); 041009.

[23] Rodriguez CV, Celis C. Design optimization methodology of small horizontal axis wind turbine blades using a hybrid CFD/BEM/GA approach. Journal of the Brazilian Society of Mechanical Sciences and Engineering 2022; 44(3): 254.

[24] Jha D, Singh M, Thakur AN. A novel computational approach for design and performance investigation of small wind turbine blade with extended BEM theory. International Journal of Energy and Environmental Engineering 2021; 12(3): 563-575.

[25] Tokul A, Kurt U. Comparative performance analysis of NACA 2414 and NACA 6409 airfoils for horizontal axis small wind turbine. International Journal of Energy Studies. 2023;8(4):879-898.

[26] Akbari V, Naghashzadegan M, Kouhikamali R, Afsharpanah F, Yaïci W. Multi-Objective Optimization and Optimal Airfoil Blade Selection for a Small Horizontal-Axis Wind Turbine (HAWT) for Application in Regions with Various Wind Potential. Machines 2022; 10(8): 687.

[27] Natarajan K, Suthakar T. Insight aerodynamic analysis on small-scale wind turbines airfoils for low Reynolds number applications. Environmental Progress & Sustainable Energy 2022; 41(4): 13807.

[28] Giguére P, Selig MS. New airfoils for small horizontal axis wind turbines. Journal of Solar Energy Engineering, Transactions of the ASME. 1998; 120(2): 108-114.

[29] Abdelwahed KS, El-Rahman A, Zhao M, Cao H, Zhang M. Aerodynamic performance prediction of SG6043 airfoil for a horizontal-axis small wind turbine. Journal of Physics: Conference Series 2020; 1452(1) :012018.

[30] Singh RK, Ahmed MR, Zullah MA, Lee YH. Design of a low Reynolds number airfoil for small horizontal axis wind turbines. Renewable Energy 2012; 42: 66-76.

[31] Noronha NP, Krishna M. Aerodynamic performance comparison of airfoils suggested for small horizontal axis wind turbines. Mater Today Proceedings 2021; 46: 2450-2455.

[32] Manwell JF, McGowan JG, Rogers AL. Wind Energy Explained: Theory, Design and Application. AJohn Wiley and Sons Ltd. Press; Chippenham, Great Britain, 2010.

[33] Koç E, Gör A. Şenel MA. Yatay Eksenli Rüzgâr Türbinlerinde Optimum Türbin Parametrelerinin Belirlenmesi-Teorik Yaklaşım. Mühendis ve Makine 57 (676):32.

[34] Maalawi KY, Badr MA. A practical approach for selecting optimum wind rotors. Renewable Energy 2003; 28(5): 803-822.

[35] Tanürün HE, Acır A. Investigation of the hydrogen production potential of the H-Darrieus turbines combined with various wind-lens. Int J Hydrogen Energy. 2022; 47(55): 23118-23138.

[36] Kaya F, Tanürün HE, Acır A. Numerical Investigation of Radius Dependent Solidity Effect on H-Type Vertical Axis Wind Turbines. Journal of Polytechnic 2022; 25(3): 1007-1019.

[37] Chen TY, Liou LR. Blockage corrections in wind tunnel tests of small horizontal-axis wind turbines. Experimental Thermal and Fluid Science 2011; 35(3): 565-569.

[38] Hsiao F Bin, Bai CJ, Chong WT. The Performance Test of Three Different Horizontal Axis Wind Turbine (HAWT) Blade Shapes Using Experimental and Numerical Methods. Energies 2013; 6(6): 2784-2803.